

An improved phase-coding method for absolute phase retrieval based on the path-following algorithm

Shenzhen Lv^{a,b}, Qiang Sun^a, Jianbai Yang^{a,b}, Yang Jiang^a, Feng Qu^a, Jian Wang^{a,*}

^a R&D Center of Precision Instruments and Equipment, Changchun Institute of Optics, Fine Mechanics & Physics, Chinese Academy of Sciences, No.3888, Dongnanhu Road, Changchun, Jilin, China

^b University of Chinese Academy of Sciences, Beijing 100049, China

ARTICLE INFO

Keywords:

Phase unwrapping
3D shape measurement
Unwrapping artifact
Path-following algorithm

ABSTRACT

Although the traditional phase-coding method for absolute phase retrieval possesses strong robustness, the method leads to unwrapping artifacts as a mass of codewords required. To solve this problem, a novel improved method is proposed in this paper. The incorrect points in the recovered phase via the traditional method are located using a computational framework, and the path-following algorithm is adopted as an aid to correct the unwrapping artifacts. The effectiveness of the proposed method is experimentally verified by an established measurement system. The reconstructed geometry of standard sphere has sufficient accuracy and the absolute phase retrieval of a complex star object has high quality.

1. Introduction

With the recent significant improvements in projection techniques and detector performance, the structured light [1–3] based 3D shape measurement technique has been rapidly developed [4–9]. Because of the merits of fast speed, high accuracy, and non-contact measurement, it has been applied in various fields [10–14], including biomedicine, computer science, and reverse engineering. As far this technique, the quality of the recovered phase from modulated sinusoidal fringe patterns is one of the determinants of measurement accuracy. There are different methods for extracting wrapped phases from captured fringe images, such as wavelet transform [13], Fourier transform [15], phase-shifting method [16], and deep learning [17], and others. The phase-shifting method is widely used in the measurement of complex 3D objects due to its fast speed and high accuracy.

The range of the wrapped phase is from 0 to 2π with discontinuities, and therefore the phase-unwrapping algorithm is required to obtain continuous phase values. The relative phase-unwrapping algorithm [18] possesses advantages of speed and convenience but is limited by the surface smooth assumption and is impractical for the simultaneous measurement of multiple separated objects. The absolute phase-unwrapping algorithms [19,20] solve the aforementioned problems by adding extra images, more hardware components, and pre-knowledge or hybrid methods such as multi-frequency [21], two wavelength [22], multi-view phase shifting [23], geometric constraint [24], phase-coding [25], and so on.

However, due to noise and sampling, all of the absolute phase-unwrapping methods lead to many different artifacts [19]. Specific methods for certain artifacts have been proposed to remove or reduce unwrapping artifacts. A valuable review in reference [19] offers some practical tips for managing the phase-unwrapping artifact issues, for example, the sparse artifact is handled by applying a median filter to locate the incorrect points and using the fringe order differences between the filtered phase and the raw phase to correct them.

The traditional phase-coding method takes advantage of a phase that is less sensitive to the noise. The maximum fringe order is determined by the number of fringe periods that could be much higher than 2^M (M is the number of binary patterns). This is compared with the gray-coding method [26,27]. However, as a large number of codewords are present in coded fringe patterns, phase-unwrapping artifacts exist near the discontinuity points of 2π . To solve this problem, Zheng and Da [28] proposed a technique by coding two phase information to generate a large number of codewords. But this method needs a total of nine fringe images for three-step phase shifting, which reduces the measurement speed. Furthermore, in the case of shape measurement of complex objects, four-step phase shifting may be required and a total of 12 fringe images are needed. Zhou et al. [29] proposed an alternative method by separately recording four-step phase-shifting fringes and phase-coding fringes into different RGB components of a color camera. However, this method cannot be applied to the shape measurement of colored objects. Xing et al. [30] applied the Newton–Raphson method to address the non-linear gamma issues of the phase-coding method if the projector's non-linear gamma was not pre-calibrated. Hyun and

* Corresponding author.

E-mail address: wangj@ciomp.ac.cn (J. Wang).

Zhang [31] proposed a novel phase-coding method requiring only five binary fringe patterns for high-speed 3D shape measurement and developed a computational framework to reduce the impact of noise on the stair phase based on the geometric constraint method.

This paper proposes a novel improved method by combining the phase-coding method with the path-following algorithm. Three-step phase-shifting technology is adopted for the measurement of complex objects, and satisfactory accuracy is achieved. Only a total of six fringe images are needed. This method includes colored objects. The methodology is described in detail and computational frameworks for single objects and spatially separated objects are provided. Experimental results for different tested objects are presented, showing the effectiveness of the proposed method.

The paper is organized as follows. Section 2 describes the principle of the proposed method. Section 3 shows the experimental results for different objects. Conclusions are drawn in Section 4.

2. Principle

2.1. The three-step phase-shifting algorithm and the N-step phase-shifting algorithm

Phase-shifting algorithms are widely used in optical metrology because of their speed and accuracy [16]. For high-speed applications, the three-step phase-shifting algorithm is the best choice since it needs the minimum number of patterns for phase recovery. The fringe patterns for a three-step phase-shifting algorithm can be mathematically written as

$$I_1(x, y) = I'(x, y) + I''(x, y) \cos(\theta - 2\pi/3), \quad (1)$$

$$I_2(x, y) = I'(x, y) + I''(x, y) \cos(\theta), \quad (2)$$

$$I_3(x, y) = I'(x, y) + I''(x, y) \cos(\theta + 2\pi/3). \quad (3)$$

where $I'(x, y)$ is the average intensity, $I''(x, y)$ is the intensity modulation, and $\theta(x, y)$ is the phase to be solved. Solving Eqs. (1)–(3) simultaneously leads to

$$\theta(x, y) = \tan^{-1} \left[\sqrt{3}(I_1 - I_2) / (2I_2 - I_1 - I_3) \right]. \quad (4)$$

For the N-step phase-shifting algorithm, the intensity of the nth image can be represented as

$$I_n(x, y) = I'(x, y) + I''(x, y) \cos(\theta(x, y) + 2n\pi/N). \quad (5)$$

Similarly, the phase of $\theta(x, y)$ can be written as

$$\theta(x, y) = -\tan^{-1} \left[\frac{\sum_{n=1}^N I_k \sin(2n\pi/N)}{\sum_{n=1}^N I_k \cos(2n\pi/N)} \right]. \quad (6)$$

Since the arctangent function only ranges from $-\pi$ to π , a phase-unwrapping algorithm is needed to remove the 2π discontinuities and obtain the absolute phase value

$$\Phi(x, y) = \phi(x, y) + 2\pi \times k(x, y), \quad (7)$$

where $\Phi(x, y)$ denotes the absolute unwrapped phase of $\phi(x, y)$ and $k(x, y)$ is an integer number called the fringe order. Essentially, the process of the phase-unwrapping method is to determine the unique k for each pixel.

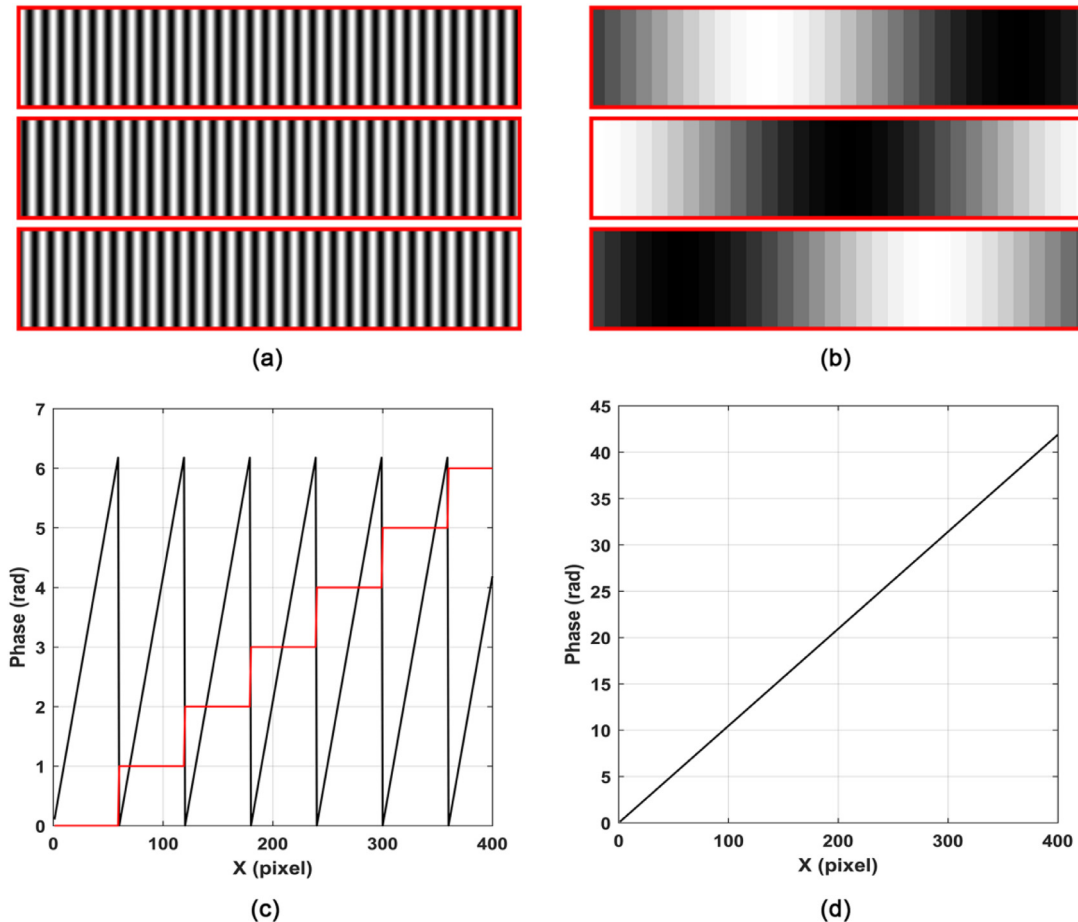


Fig. 1. Schematic diagram of the phase-coding method. (a) The sinusoidal fringe patterns ($T = 60$ pixels) for the three-step phase-shifting algorithm. (b) The encoded fringe patterns. (c) The 2π discontinuities of the wrapped phase precisely aligned as the change in the stair phase. (d) The absolute unwrapped phase.

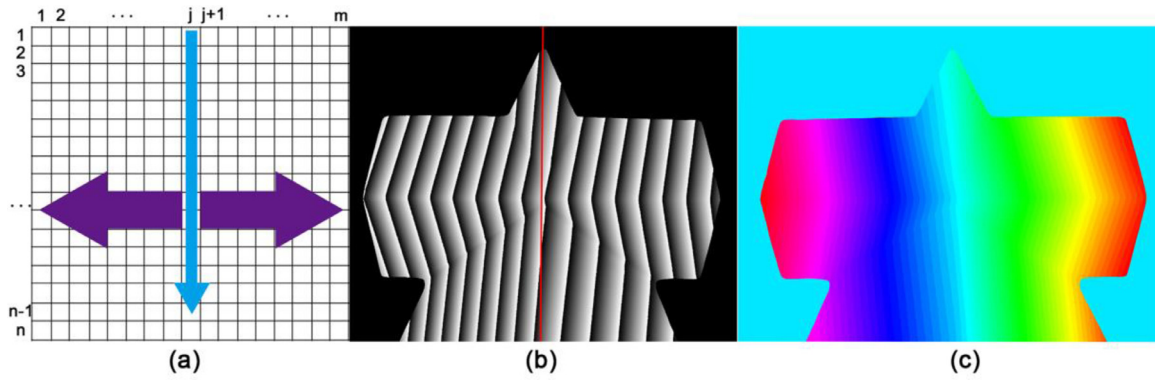


Fig. 2. The relative phase-unwrapping method. (a) Schematic diagram of the path-following method. (b) The wrapped phase of the plaster star object in which the pixels of the red line are selected as the initial column. (c) The relative unwrapped phase with the pixels of the red line as the initial column. (For interpretation of the references to color in this figure legend, the reader is referred to the web version of this article.)

2.2. Phase-coding method

Essentially, the phase-coding method [25] determines the fringe orders using the stair phase perfectly aligned with the 2π discontinuities. Since each stair is unique, the stair information can be treated as a codeword for the k value. Fig. 1 shows a schematic diagram of the phase-coding method with (a) the presence of sinusoidal fringe patterns ($T=60$ pixels) for the three-step phase-shifting algorithm. The phase of the encoded fringe pattern can be described as

$$\vartheta^s(x, y) = \text{floor}\left(\frac{x}{T}\right) \times \frac{2\pi}{N}, \quad (8)$$

where floor () is the truncated integer, the s superscript denotes the stair phase, T is the fringe pitch, and N is the total number of fringe periods.

The encoded fringe pattern as shown in Fig. 1(b) can be written as

$$I_k = I'(x, y) + I''(x, y)\cos(\vartheta^s(x, y) + \delta_k), \quad (9)$$

where the phase shift values of δ_k are $-\frac{2\pi}{3}$, 0 , and $\frac{2\pi}{3}$.

Fig. 1(c) shows that the 2π discontinuities of the wrapped phase are precisely aligned with the change in the stair phase. Using the stair phase information, the fringe orders can be determined by

$$k = \text{round}\left(\frac{N\vartheta^s}{2\pi}\right). \quad (10)$$

Fig. 1(d) shows the absolute phase recovered by Eq. (7).

2.3. Path-following method

The spatial phase-unwrapping method can be classified into path-following method and minimum norm method categories [32]. The path-following method seeks the integration result that is independent of the path. The minimum norm method seeks the minimum norm of the error that is independent of the path. In this study, the relative phase is recovered using the path-following method because the minimum norm method is limited by boundary conditions. As shown in Fig. 3(c) and (d), when the fringes are not full, errors occur. The main process of the method is as follows. First, we unwrap the phase vertically along a column of the tested object, and then unwrap the phase along each row with the unwrapped phase as the initial value. Fig. 2(a) shows a schematic diagram of the path-following method process. The j th column of the wrapped phase shown with the blue arrow is unwrapped by the rules as follows

$$\delta = \varphi(i, j) - \varphi(i-1, j)$$

$$\Phi(i, j) = \begin{cases} \varphi(1, j) & \text{when } i = 1 \\ \Phi(i-1, j) + \delta & \text{if } (\text{abs}(\delta) < \pi) \text{ when } i \geq 2. \\ \Phi(i-1, j) + \delta + 2\pi & \text{else if } (\delta < 0) \text{ when } i \geq 2 \\ \Phi(i-1, j) + \delta - 2\pi & \text{else when } i \geq 2 \end{cases} \quad (11)$$

Then each row of the wrapped phase, shown as the purple arrow, is unwrapped with the j th column phase as the initial value. The unwrapping rules are similar to those previously described. In this study, the selected initial column should be on the tested object and the unwrapping is along two opposite directions of the row. A proper selection of the initial column is important especially for complex objects such as a plaster star as shown in Fig. 2(b), where the initial column is represented by a red line. Fig. 2(c) demonstrates the relative unwrapped phase distribution via the path-following algorithm used in this study.

2.4. Computational framework of the improved phase-coding method

This section describes the framework of the improved phase-coding method as follows. To illustrate framework more easily, without losing generality, we adopt a single plaster ball as shown in Fig. 3(a) as the tested object.

Step 1: Segmentation of the object regions using image-processing techniques

We create a mask image for the plaster ball from the texture image by image segmentation proposed in references [33] and [34], which is shown in Fig. 3(b). Then the sinusoidal fringe patterns and encoded fringe patterns can be extracted using the mask. Fig. 3(c) and (d) show the extracted sinusoidal fringe and encoded fringe patterns, respectively.

Step 2: The wrapped phase and absolute phase recovery

The wrapped phase and the absolute phase of the plaster ball are extracted using Eq. (4) and the phase-coding method described in Section 2.2., respectively. The acquired phase maps are shown in Fig. 3(e) and (f). There are many incorrect points around 2π discontinuities for in the absolute phase map of Fig. 3(f), which can be easily found from a zoom-in view of the map.

Step 3: Location of incorrect points in the absolute phase

We first locate the incorrect points in the absolute phase using Canny filtering. The result is shown in Fig. 3(g). Then we extend the incorrect points for several surrounding pixels using a Wiener filter [35] to detect some incorrect points. Fig. 3(h) shows the extending results. This method of locating incorrect points in the absolute phase is also applicable to binary coding, gray coding, and two-wavelength phase unwrapping.

Step 4: Relative phase unwrapping

Fig. 3(i) shows the relative unwrapped phase acquired using the path-following method described in Section 2.3. The relative unwrapped phase is a continuous phase starting from a point on the tested object. There is a relationship between the relative unwrapped phase and the absolute unwrapped phase, which can be

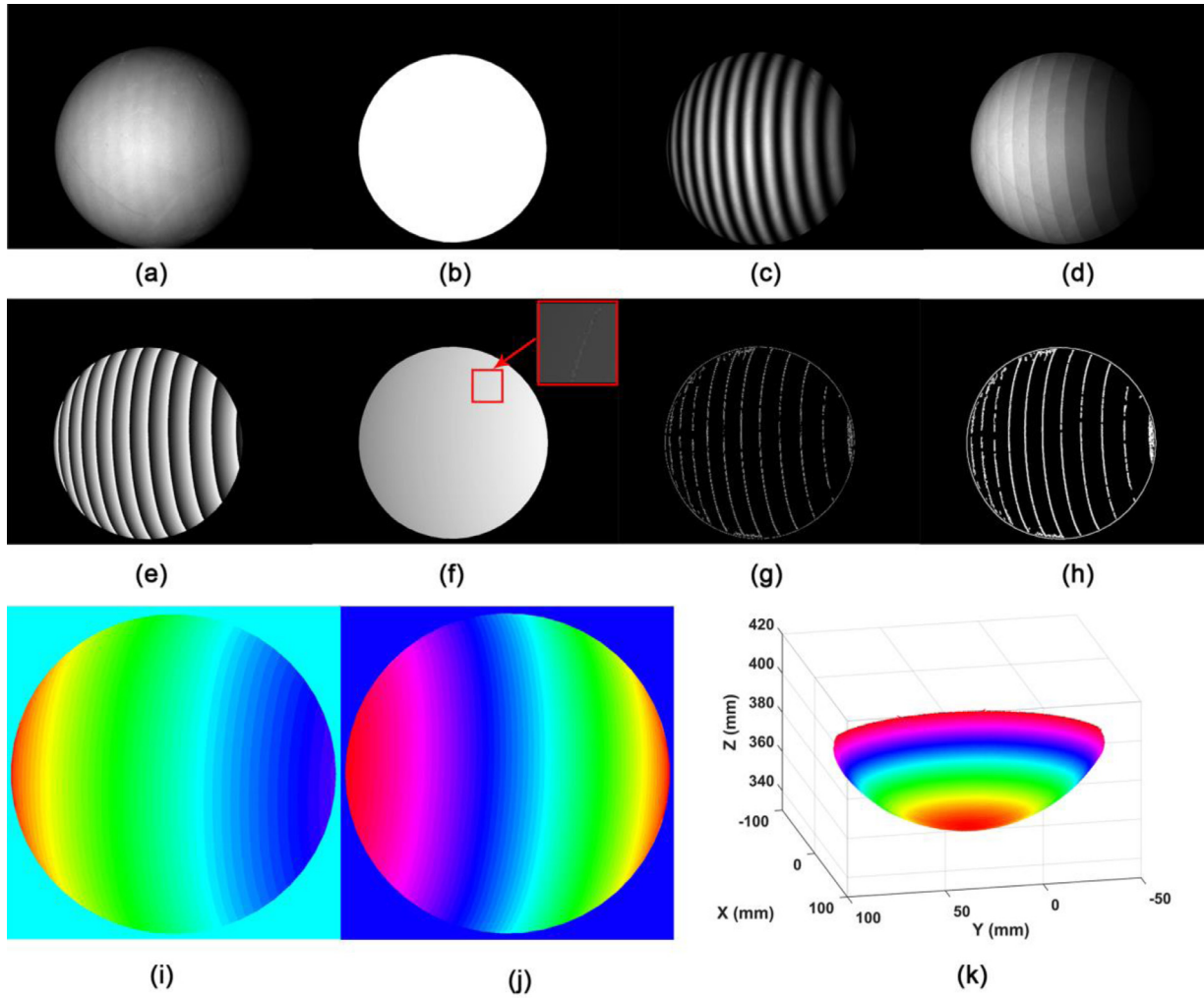


Fig. 3. The computational framework of the improved phase-coding method. (a) A plaster ball is used as the tested object. (b) The mask image of the ball acquired via edge extraction and image segmentation. (c) One of the sinusoidal fringe patterns in the phase-shifting algorithm extracted using the mask. (d) One of the phase-encoded fringe patterns extracted using the mask. (e) Diagram of the acquired wrapped phase of the ball using Eq. (4). (f) Diagram of the acquired absolute phase of the ball using the traditional phase-encoding method. (g) Positions of the incorrect points in the absolute phase diagram extracted via Canny filtering. (h) Extension of the incorrect points for several surrounding pixels using the Wiener filter. (i) Diagram of the relative unwrapped phase solved using the path-following method. (j) The absolute phase diagram unwrapped using the improved phase-encoding algorithm. (k) 3D information on the reconstructed plaster ball using the proposed method.

expressed as

$$\Phi_{abs} = \Phi_{rel} + \Delta\Phi, \quad (12)$$

where Φ_{abs} represents the absolute phase, Φ_{rel} denotes the relative wrapped phase, and $\Delta\Phi$ is a constant to be determined.

Step 5: Determination of $\Delta\Phi$

First, we calculate the differences between the absolute phase in Fig. 3(f) and the relative phase in Fig. 3(i), except for the incorrect points in Fig. 3(h). Then $\Delta\Phi$ can be obtained by calculating the average of the differences.

Step 6: The final absolute phase recovery

The corrected absolute phase can be obtained using Eq. (12). The unwrapped phase of the plaster ball is obtained as shown in Fig. 3(j).

2.5. Calibration of the structured light system

In this study, the camera is a pinhole model. The relationship between a point of (x^w, y^w, z^w) on the object and its projection on the image sensor of (u^c, v^c) can be written as

$$s^c \begin{bmatrix} u^c & v^c & 1 \end{bmatrix}^T = M^c \begin{bmatrix} x^{tw} & y^{tw} & z^{tw} & 1 \end{bmatrix}^T, \quad (13)$$

$$M^c = A^c \begin{bmatrix} R^c & t^c \end{bmatrix}, \quad (14)$$

where the c superscript denotes the camera's parameters, s^c is a scale factor, A^c is the camera's intrinsic matrices, and R^c and t^c are the camera's extrinsic matrices describing the process of rotation and translation, respectively. The projector can be regarded as an inverse camera [36]. There is a similar relationship between the point and its projection on the projector sensor

$$s^p \begin{bmatrix} u^p & v^p & 1 \end{bmatrix}^T = M^p \begin{bmatrix} x^{tw} & y^{tw} & z^{tw} & 1 \end{bmatrix}^T, \quad (15)$$

$$M^p = A^p \begin{bmatrix} R^p & t^p \end{bmatrix}, \quad (16)$$

where the p superscript denotes the parameters of the projector.

This study adopts the system calibration methods proposed in references [37,38]. First, 10 different pose images of a circle board are captured to establish the intrinsic parameters of the camera using the MATLAB toolbox. Since the projector cannot capture images like the camera, the correspondence between the camera pixel and the projector pixel must be established using the absolute gradient phase maps along

both the horizontal and vertical directions. Then the circle centers on the projector sensor can be written as

$$u^p = \frac{\Phi^V(u^c, v^c)}{2\pi} T_1, \quad (17)$$

$$v^p = \frac{\Phi^H(u^c, v^c)}{2\pi} T_1, \quad (18)$$

where Φ^V and Φ^H are the absolute phase maps along the vertical and horizontal directions, respectively, and T is the fringe period of the narrowest fringe pattern. In this study, the absolute phase maps for the calibration of the structured light system are recovered using the multi-frequency phase-shifting algorithm, which has nine-step phase-shifted fringe patterns for the narrowest fringe pattern ($T_1 = 21$ pixels) and additional sets of five-step phase-shifted fringe patterns for the wider fringe patterns ($T_2 = 24$ pixels and $T_3 = 180$ pixels). Thus, the intrinsic parameters of the projector are obtained.

The extrinsic parameters are estimated using the MATLAB stereo calibration toolbox. When the intrinsic and extrinsic parameters of the system are acquired, four equations about 3D information on the object can be obtained using Eqs. (13) and (15), and any three of them are sufficient for the 3D shape measurement. However, there is an optimal fringe angle for the 3D shape reconstruction [39]. Our experiments demonstrated

that the vertical fringe patterns perform better than the horizontal fringe patterns with the developed system. Then the 3D shape reconstruction can be written as

$$\begin{bmatrix} x^w & y^w & z^w \end{bmatrix}^T = (H^T H)^{-1} H^T b, \quad (19)$$

with

$$H = \begin{bmatrix} M^c(1,1) - u^c M^c(3,1) & M^c(1,2) - u^c M^c(3,2) & M^c(1,3) - u^c M^c(3,3) \\ M^c(2,1) - u^c M^c(3,1) & M^c(2,2) - u^c M^c(3,2) & M^c(2,3) - u^c M^c(3,3) \\ M^p(1,1) - u^p M^p(3,1) & M^p(1,2) - u^p M^p(3,2) & M^p(1,3) - u^p M^p(3,3) \end{bmatrix}$$

and

$$b = [u^c M^c(3,4) - M^c(1,4) \quad v^c M^c(3,4) - M^c(2,4) \quad u^p M^p(3,4) - M^p(1,4)]^T,$$

where $M^c(i, j)$ and $M^p(i, j)$ are the matrix elements in the i th row and j th column of the camera and projector, respectively. Fig. 3(k) shows the 3D shape information on the reconstructed plaster ball using this calibration and reconstruction method.

3. Experiments

The structured light based 3D shape measurement system consists of a CCD camera (DAHENG MER-131-210U3M-L) and a projector (DLP VisionFly 6500). The camera has a focal length of 10 mm, resolution of 1024×1280 pixels, and sensor unit size of $4.8 \mu\text{m} \times 4.8 \mu\text{m}$. The projector

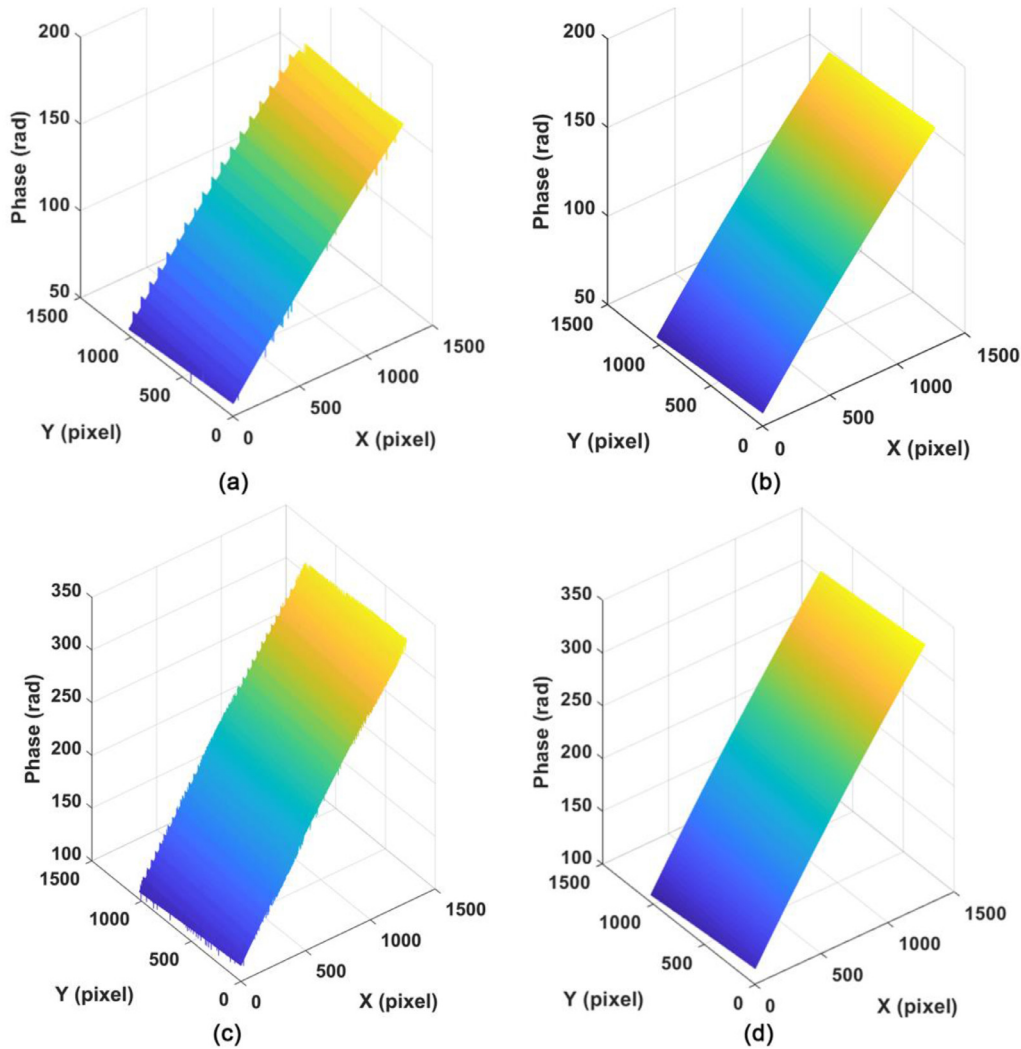


Fig. 4. Comparison of the phase-coding method and the proposed method. (a) The recovered phase for $T=60$ pixels and $N=32$ using the phase-coding method. (b) The corrected phase for $T=60$ pixels and $N=32$ using the proposed method. (c) The recovered phase for $T=30$ pixels and $N=64$ using the phase-coding method. (d) The corrected phase for $T=30$ pixels and $N=64$ using the proposed method.

has a focal length of 23 mm, resolution of 1080×1920 pixels, and sensor unit size of $7.6 \mu\text{m} \times 7.6 \mu\text{m}$.

First, we demonstrate the serious phase-unwrapping errors around the 2π discontinuities of the phase using the traditional phase-coding method when a large number of codewords (such as $N=32, 64\dots$) is adopted. In the experiments, we project sinusoidal fringe patterns and coded fringe patterns with periods of 60 pixels ($N=32$) onto a white board as shown in Fig. 1(a) and (b) and synchronously capture these patterns using the camera. The absolute phase is then recovered using the phase-coding method. The result is shown in Fig. 4(a). Obviously, there are many error points around the 2π discontinuities that must be corrected. We repeat the experiment with the period of the fringe patterns set at 30 pixels ($N=64$). The recovered absolute phase is shown in Fig. 4(c). There are also obvious error points around the 2π discontinuities of the phase. Then we perform absolute phase unwrapping of the white board with the computational framework described in Section 2 of this paper. Fig. 4(b) shows the experimental result of the corrected absolute phases with a fringe period of 60 pixels. Fig. 4(d) shows the result with a fringe period of 30 pixels. The unwrapped absolute phases are well corrected using the proposed method. Since the tested object is a

flat white board and a mask is unnecessary, the computation can start with the second step of the framework.

To further examine the superiority of the performance of the proposed method, we compare the three-frequency phase-shifting algorithm as follows. It is well known that more phase-shifted fringe patterns result in a more accurate recovered phase. Therefore, we adopt nine-, five-, and five-step phase-shifting technology for the first, second, and third frequencies in the algorithm, respectively, to achieve a sufficiently accurate phase recovery. Fig. 5(a) shows the recovered phase when the T1, T2, and T3 fringe pattern periods are 60, 80, and 270 pixels, respectively. These fringe pattern periods result in a final equivalent fringe period of T with a value of 2160 pixels, which is greater than the number of projector pixels along the horizontal direction. With the data of the corrected phase in Fig. 4(b) and the recovered phase in Fig. 5(a), we can obtain the difference between the two phase diagrams along a row. The result is shown in Fig. 5(b). The rms value of the differences in Fig. 5(b) is 0.0296 rad, proving the effectiveness of the proposed method. Fig. 5(c) shows the recovered phase when the T1, T2, and T3 fringe pattern periods are 30, 35, and 230 pixels, respectively. The final equivalent fringe period of T is also greater than the number of projector pixels, with a value of 2415 pixels. With the data from Figs. 4(b) and 5(c), the differ-

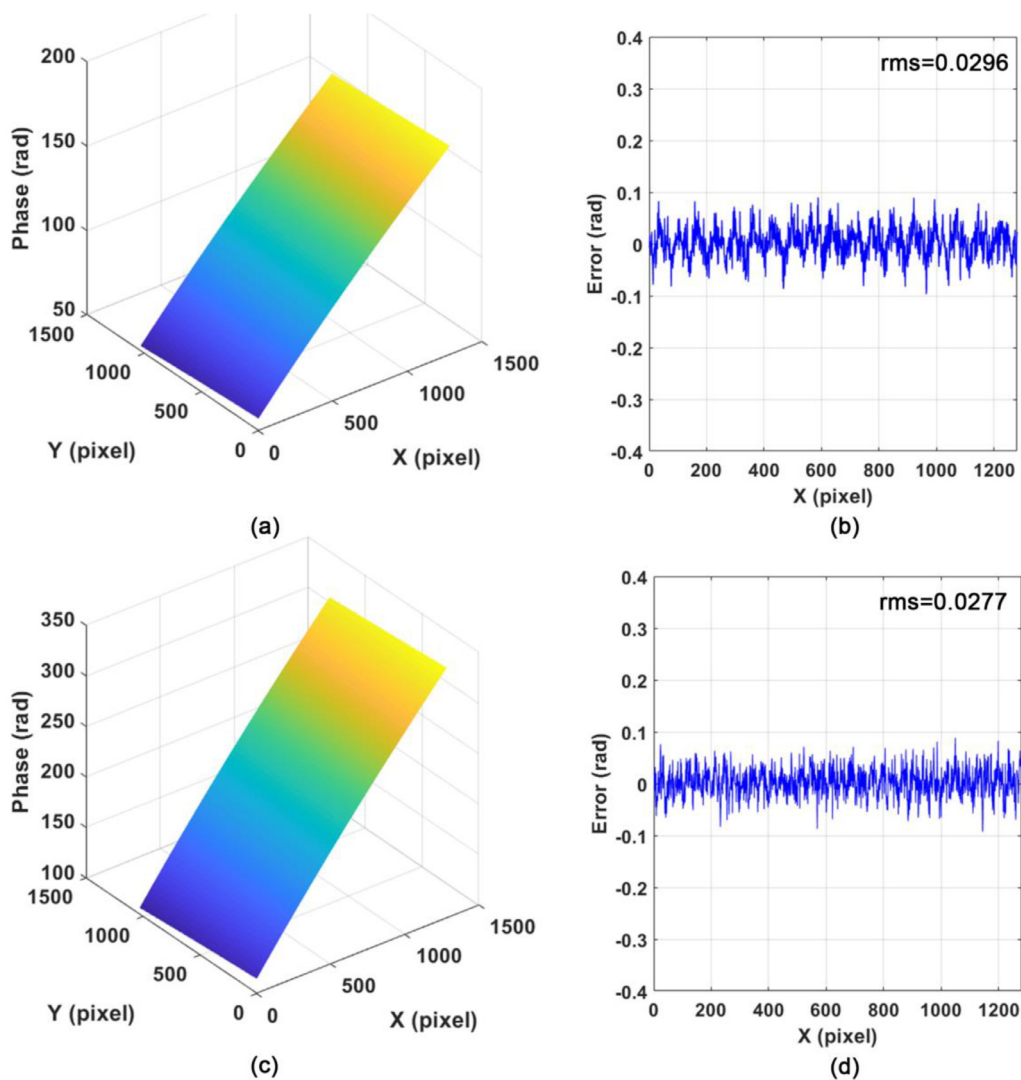


Fig. 5. Comparison of the proposed method and the multi-frequency phase-shifting algorithm. (a) The recovered phase of the fringe patterns with T1 = 60 pixels, T2 = 80 pixels, and T3 = 270 pixels using the multi-frequency phase-shifting algorithm; a row of the difference between the proposed and multi-frequency phase-shifting algorithm (rms = 0.0296 rad). (c) The recovered phase of the fringe patterns with T1 = 30 pixels, T2 = 35 pixels, and T3 = 230 pixels using the multi-frequency phase-shifting algorithm. (d) A row of the difference between the proposed method and the multi-frequency phase-shifting algorithm (rms = 0.0277 rad).

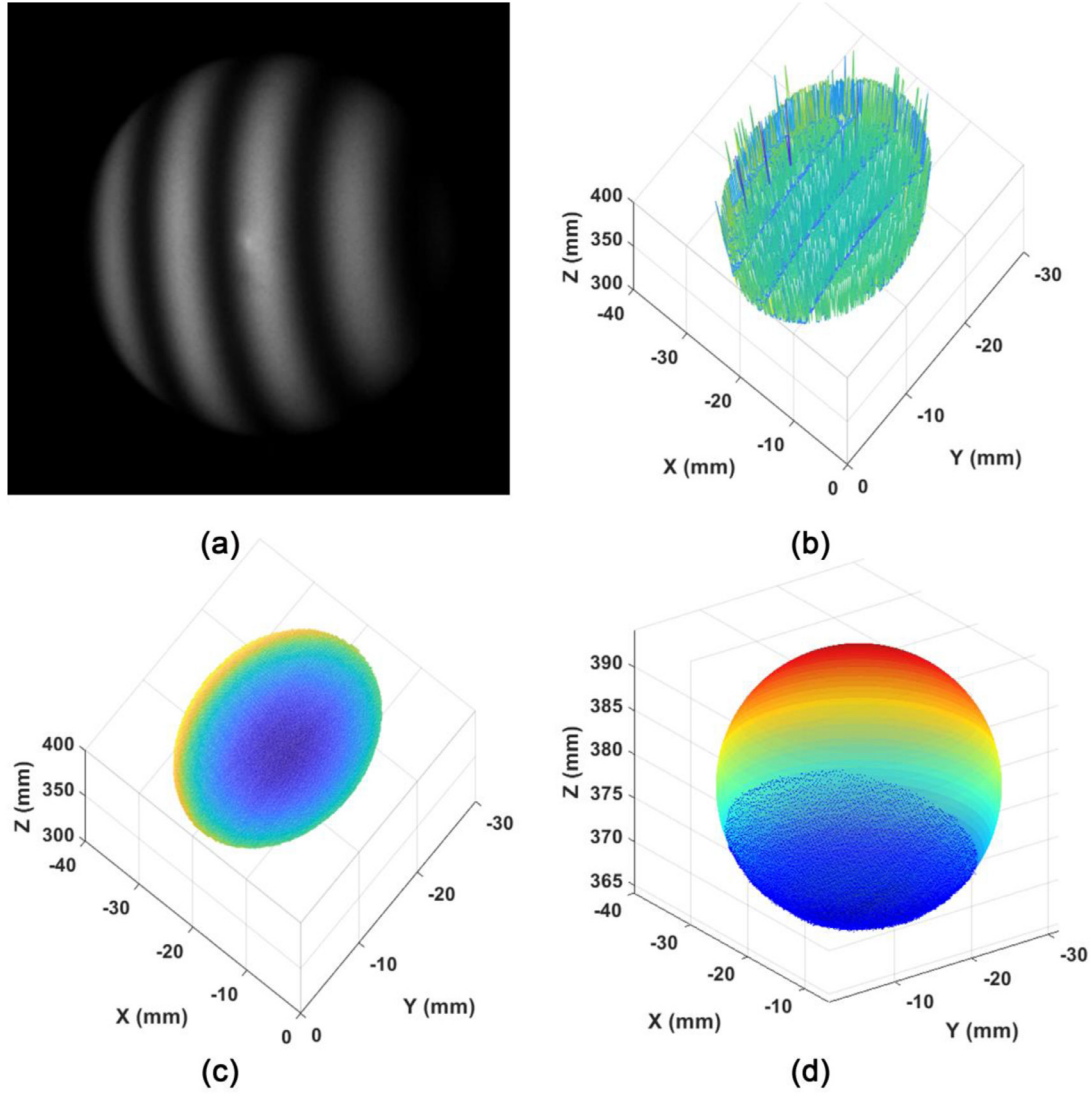


Fig. 6. Experimental results of the 3D shape measurement of a matt ceramic spherical object with fringe periods of 30 pixels ($N=64$). (a) The tested matt ceramic spherical object. (b) Reconstructed 3D geometry of the object using the traditional phase-coding method. (c) Reconstructed 3D geometry of the object using the proposed method. (d) The fitting results with the blue points obtained using the point cloud measurement data. The radius of the fitted sphere is 14.9354 mm with an rms of 0.0885 mm and an error of -0.0699 mm.

ence between the two phase diagrams along a row is obtained as shown in Fig. 5(d). The rms value of the differences in Fig. 5(d) is 0.0277 rad in this case.

We measure the three-dimensional shape of a matt ceramic spherical object by separately applying the traditional phase-coding method and the proposed method. The spherical object is specially manufactured and has a diameter of 30.0105 mm and a sphericity of 0.002 mm. The intrinsic and extrinsic parameter matrices of the established measurement system are acquired using the method given in Section 2 of this paper and can be written as

$$A^c = \begin{bmatrix} 2160.007 & 0 & 654.592 \\ 0 & 2160.274 & 492.456 \\ 0 & 0 & 1 \end{bmatrix},$$

$$A^p = \begin{bmatrix} 3068.800 & 0 & 1012.686 \\ 0 & 3067.842 & 576.259 \\ 0 & 0 & 1 \end{bmatrix}.$$

$$R^c = \begin{bmatrix} 1 & 0 & 0 \\ 0 & 1 & 0 \\ 0 & 0 & 1 \end{bmatrix}, r^c = \begin{bmatrix} 0 \\ 0 \\ 0 \end{bmatrix},$$

$$R^p = \begin{bmatrix} 3068.800 & 0 & 1012.686 \\ 0 & 3067.842 & 576.259 \\ 0 & 0 & 1 \end{bmatrix}, r^p = \begin{bmatrix} 118.713 \\ -1.741 \\ 296.767 \end{bmatrix}.$$

The 3D geometry of the tested object can be reconstructed according to Eq. (19). Fig. 6(b) and (c) show the experimental results using the traditional phase-coding method and the proposed method, respectively. The reconstructed geometry using the proposed method is more accurate and smoother than that of the traditional phase-coding method. We can then perform spherical fitting using the measurement point data obtained via the proposed method. The fitted result is shown in Fig. 6(d). The blue points below are provided by the point cloud data of the measurement and the colored transparent ball is the fitting result. The fitted spherical equation can be written as

$$x^2 + y^2 + z^2 + 41.5045x + 32.8332y - 758.6521z + 14436.5364 = 0. \quad (20)$$

The radius of the fitted sphere is 14.9354 mm with an rms value of 0.0885 mm and an error of -0.0699 mm. The radius of the fitted sphere by the traditional phase-coding method is 12.9043 mm with an rms value of 3.6357 mm and an error of -2.101 mm.

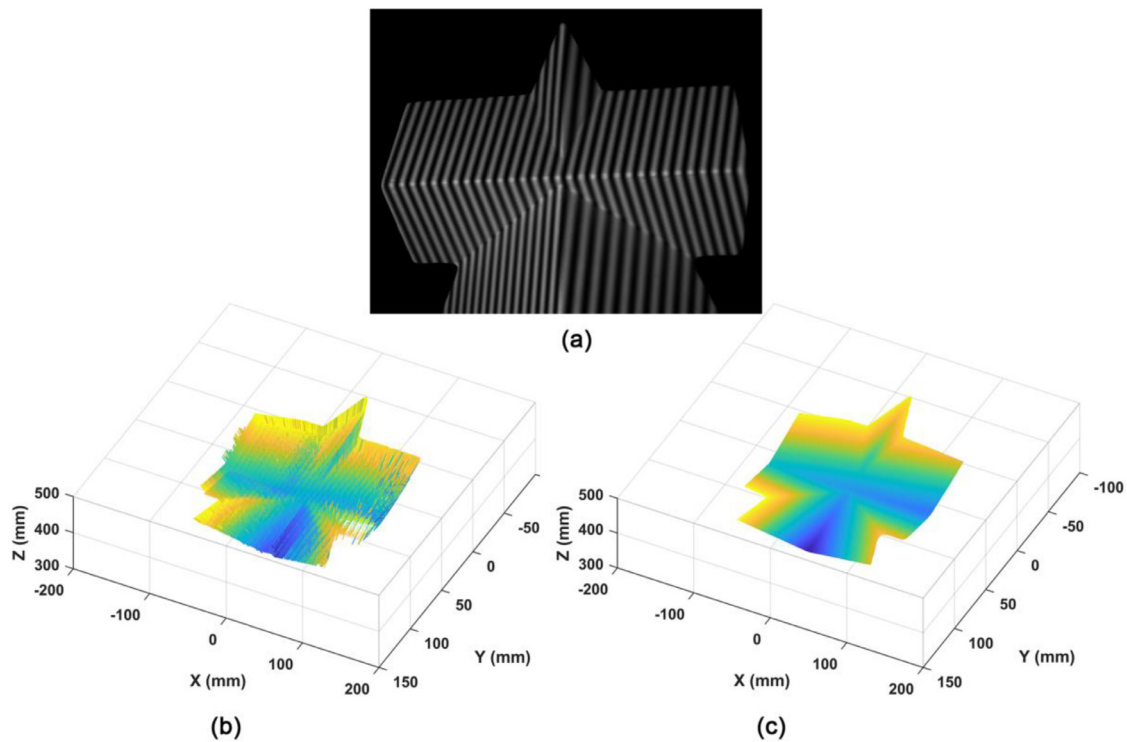


Fig. 7. 3D shape measurement of the star object with a fringe period of 30 pixels ($N=64$). (a) Star object image. (b) 3D shape reconstruction result using the traditional phase-coding method. (c) 3D shape reconstruction result using the proposed method.

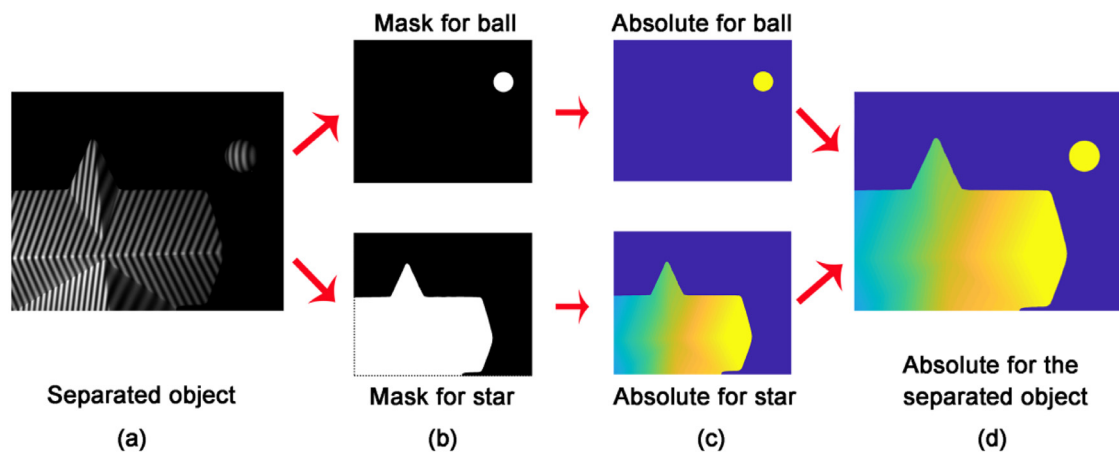


Fig. 8. Flow process diagram of the absolute phase retrieval for the separated objects. (a) The tested objects are a star and a standard sphere. (b) Two masks acquired using image processing techniques. (c) The corrected absolute phase distribution for each of the separated objects. (d) The whole absolute phase of the tested object acquired by integrating the phase distributions in (c).

The experimental results prove that the high-precision measurement of objects can be achieved using the improved phase-coding method.

To further demonstrate the validity of 3D shape reconstruction using the proposed method, the complex star object shown in Fig. 7(a) is measured. The phase-coding fringe pattern period is set at 30 pixels ($N=64$). Fig. 7(b) and (c) show the measurement results using the traditional phase-coding method and the proposed method, respectively. There are many reconstruction errors in Fig. 7(b), and these errors obviously disappear in Fig. 7(c). The high quality of the 3D shape reconstruction in Fig. 7(c) illustrates that the proposed method performs well in the shape measurement of complex objects. A prerequisite is needed using the proposed method. The tested object surface geometry should not introduce more than π phase differences between two successive points.

The simultaneous 3D shape measurement of two separated objects using the proposed method is then carried out. The tested objects are a star and a standard sphere, and the period of the fringe patterns is 30 pixels ($N=64$) as shown in Fig. 8(a). For the segmentation of the object regions, two masks are created, one for the star and one for the ball as shown in Fig. 8(b). Then the simultaneous measurement of two separated objects can be treated as two separated measurements of the objects. The corrected absolute phase for each of the objects is obtained using the computational framework given in Section 2 and is demonstrated in Fig. 8(c). The whole absolute phase distribution of the tested object is acquired by simply integrating the two absolute phase distributions together as shown in Fig. 8(d). Combining the calibration results of the measurement system the 3D shape reconstruction of the tested object is achieved and is shown in Fig. 9. The reconstruction is smooth

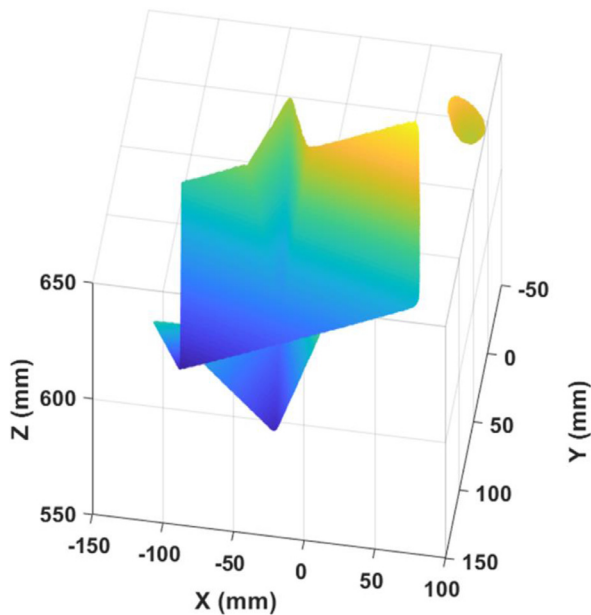


Fig. 9. The 3D shape reconstruction of the tested object.

and without error points, demonstrating the validity of the simultaneous measurement of multiple objects.

4. Conclusions

This paper proposes a novel method for improving the quality of the absolute phase retrieval when a mass of codewords is required in the phase-coding procedure. A computational framework to locate incorrect phase-unwrapping points via image processing is described and the corrected absolute phase is achieved based on the path-following algorithm. This computational framework is applicable not only for phase-encoding, but also for binary coding and gray coding.

We demonstrate that the error points around the 2π discontinuities of the recovered absolute phase obtained via the traditional phase-coding method are well corrected using this method. The accuracy of the phase retrieval can be as high as that acquired by the three-frequency phase-shifting algorithm, which requires a total of 19 fringe patterns. For a standard spherical object with a diameter of 30.0105 mm, the reconstructed sphere has a radius error of only -0.0699 mm, and for a complex star object, the reconstructed star has satisfactory quality compared with the traditional phase-coding method. A computational framework of the simultaneous measurement of multiple objects is also presented. The experimental result demonstrates the validity of the proposed method.

Finally, compared with other improved phase-coding methods, this study used only six fringe patterns and there were no restrictions on the colors of the tested objects.

Funding

This work was supported by the Scientific Instrument Developing Project of the Chinese Academy of Sciences [YJKYYQ20180067].

References

- [1] Gorthi SS, Rastogi P. Fringe projection techniques: whither we are? *Opt Laser Eng* 2010;48(2):133–40.
- [2] Zhang S. Recent progresses on real-time 3D shape measurement using digital fringe projection techniques. *Opt Laser Eng* 2010;48(2):149–58.
- [3] Geng J. Structured-light 3D surface imaging: a tutorial. *Adv Opt Photon* 2011;3(2):128–60.

- [4] Zuo C, Tao T, Feng S, Huang L, Asundi A, Chen Q. Micro Fourier Transform Profilometry (μ FTP): 3D shape measurement at 10,000 frames per second. *Opt Laser Eng* 2018;102:70–91.
- [5] Heist S, Dietrich P, Landmann M, Kuhmstedt P, Notni G, Tunnermann A. GOBO projection for 3D measurements at highest frame rates: a performance analysis. *Light Sci Appl* 2018;7:71.
- [6] Qian J, Tao T, Feng S, Chen Q, Zuo C. Motion-artifact-free dynamic 3D shape measurement with hybrid Fourier-transform phase-shifting profilometry. *Opt Express* 2019;27(3):2713–31.
- [7] Heist S, Lutzke P, Schmidt I, Dietrich P, Kühmstedt P, Tünnermann A, Notni G. High-speed three-dimensional shape measurement using GOBO projection. *Opt Laser Eng* 2016;87:90–6.
- [8] Zhang S. High-speed 3D shape measurement with structured light methods: a review. *Opt Laser Eng* 2018;106:119–31.
- [9] Su X, Zhang Q. Dynamic 3-D shape measurement method: a review. *Opt Laser Eng* 2010;48(2):191–204.
- [10] Heist S, Zhang C, Reichwald K, Kuhmstedt P, Notni G, Tunnermann A. 5D hyperspectral imaging: fast and accurate measurement of surface shape and spectral characteristics using structured light. *Opt Express* 2018;26(18):23366–79.
- [11] Flores J, Stronik M, Munoz A, Garcia-Torales G, Ordoñez S, Cruz A. Dynamic 3D shape measurement by iterative phase shifting algorithms and colored fringe patterns. *Opt Express* 2018;26(10):12403–14.
- [12] Li C, Li Y, Xiao Y, Zhang X, Tu D. Phase measurement deflectometry with refraction model and its calibration. *Opt Express* 2018;26(26):33510–22.
- [13] Inanç A, Kösoğlu G, Yüksel H, Naci İnci M. 3-D optical profilometry at micron scale with multi-frequency fringe projection using modified fibre optic Lloyd's mirror technique. *Opt Laser Eng* 2018;105:14–26.
- [14] Feng S, Chen Q, Zuo C, Asundi A. Fast three-dimensional measurements for dynamic scenes with shiny surfaces. *Opt Commun* 2017;382:18–27.
- [15] Lohry W, Zhang S. Fourier transform profilometry using a binary area modulation technique. *Opt Eng* 2012;51(11):113602.
- [16] Malacara D, editor. *Optical shop testing*. 3rd ed.. New York, NY: John Wiley and Sons; 2007.
- [17] Rivenson Y, Zhang Y, Günaydin H, Teng D, Ozcan A. Phase recovery and holographic image reconstruction using deep learning in neural networks. *Light* 2018;7(2):e17141.
- [18] Su X, Chen W. Reliability-guided phase unwrapping algorithm: a review. *Opt Laser Eng* 2004;42(3):245–61.
- [19] Zhang S. Absolute phase retrieval methods for digital fringe projection profilometry: a review. *Opt Laser Eng* 2018;107:28–37.
- [20] Zuo C, Huang L, Zhang M, Chen Q, Asundi A. Temporal phase unwrapping algorithms for fringe projection profilometry: a comparative review. *Opt Laser Eng* 2016;85:84–103.
- [21] Cheng Y-Y, Wyant JC. Multiple-wavelength phase-shifting interferometry. *Appl Opt* 1985;23:804–7.
- [22] Servin M, Padilla M, Garmica G. Super-sensitive two-wavelength fringe projection profilometry with 2-sensitivities temporal unwrapping. *Opt Laser Eng* 2018;106:68–74.
- [23] Li Z, Zhong K, Li Y, Zhou X, Shi Y. Multiview phase shifting: a full-resolution and high-speed 3D measurement framework for arbitrary shape dynamic objects. *Opt Lett* 2013;38(9):1389–91.
- [24] Hyun J, Zhang S. Enhanced two-frequency phase-shifting method. *Appl Opt* 2016;55(16):4395–401.
- [25] Wang Y, Zhang S. Novel phase-coding method for absolute phase retrieval. *Opt Lett* 2012;37:2067–9.
- [26] Zhang Q, Su X, Xiang L, Sun X. 3-D shape measurement based on complementary Gray-code light. *Opt Laser Eng* 2012;50(4):574–9.
- [27] Zheng D, Da F. Self-correction phase unwrapping method based on Gray-code light. *Opt Laser Eng* 2012;50(8):1130–9.
- [28] Zheng D, Da F. Phase coding method for absolute phase retrieval with a large number of codewords. *Opt Express* 2012;20:24139–50.
- [29] Zhou C, Liu T, Si S, Xu J, Liu Y, Lei Z. An improved stair phase encoding method for absolute phase retrieval. *Opt Laser Eng* 2015;66:269–78.
- [30] Xing Y, Quan C, Tay C. A modified phase-coding method for absolute phase retrieval. *Opt Laser Eng* 2016;87:97–102.
- [31] Hyun J, Zhang S. Superfast 3D absolute shape measurement using five binary patterns. *Opt Laser Eng* 2017;90:217–24.
- [32] Ghiglia DC, Pritt MD, editors. *Two-dimensional phase unwrapping: theory, algorithms, and software*. New York: John Wiley and Sons; 1998.
- [33] Li B, Zhang S. Superfast high-resolution absolute 3D recovery of a stabilized flapping flight process. *Opt Express* 2017;25(22):27270–82.
- [34] Dai J, An Y, Zhang S. Absolute three-dimensional shape measurement with a known object. *Opt Express* 2017;25(9):10384–96.
- [35] Zhang S. Composite phase-shifting algorithm for absolute phase measurement. *Opt Laser Eng* 2012;50(11):1538–41.
- [36] Zhang S, Huang P. Novel method for structured light system calibration. *Opt Eng* 2006;45(8):083601–8.
- [37] Li B, Karpinsky N, Zhang S. Novel calibration method for structured-light system with an out-of-focus projector. *Appl Opt* 2014;53(16):3415–26.
- [38] Li Z, Shi Y, Wang C, Wang Y. Accurate calibration method for a structured light system. *Opt Eng* 2008;47(5):0536041–9.
- [39] Li B, Zhang S. Structured light system calibration method with optimal fringe angle. *Appl Opt* 2014;53(33):7942–50.